ICESat-2 Onboard Flight Receiver Algorithms: On-orbit Parameter Updates the Impact on Science Driven Observations

Lori Magruder[1], Ann Rackley Reese[2,3], Aimée Gibbons[2,3] James Dietrich[1] and Tom Neumann[3]

[1]Center for Space Research, University of Texas at Austin, Austin, TX.

[2]KBR, Greenbelt, MD

[3]NASA Goddard Space Flight Center, Greenbelt, MD

Corresponding author: Lori Magruder[†] (lori.magruder@austin.utexas.edu)

Key Points:

- Since the 2018 ICESat-2 launch multiple updates have been made to the satellite's onboard flight receiver algorithm parameters to improve access and utility of the data for a multi-disciplinary science community
- The adjustments have been primarily in the in the vertical telemetry window settings and have facilitated enhanced observations of blowing snow and increased detection opportunities of bathymetry in nearshore environments
- The parameter changes have been made to mitigate data losses in certain situations and to advance science applications outside of the primary science objectives of the ICESat-2 mission.

Abstract

The ICESat-2 (Ice, Cloud and Land Elevation Satellite-2) photon-counting laser altimeter technology required the design and development of very sophisticated onboard algorithms to collect, store and downlink the observations. These algorithms utilize both software and hardware solutions for meeting data volume requirements and optimizing the science achievable via ICESat-2 measurements. Careful planning and dedicated development were accomplished during the pre-launch phase of the mission in preparation for the 2018 launch. Once on-orbit all of the systems and subsystems were evaluated for performance, including the receiver algorithms, to ensure compliance with mission standards and satisfy the mission science objectives. As the mission has progressed and the instrument performance and data volumes were better understood, there have been several opportunities to enhance ICESat-2's contributions to earth observation science initiated by NASA and the ICESat-2 science community. We highlight multiple updates to the flight receiver algorithms, the onboard software for signal processing, that have extended ICESat-2's data capabilities and allowed for advanced science applications beyond the original mission objectives.

Plain Language Summary

NASA launched its second Earth observing laser altimeter in 2018 with mission objectives of collecting observations in support of Earth science as a window into climate change impacts on our planet. Pre-launch studies focused on specific instrument settings and on-board data processing to support the mission objectives without violating data volume constraints. Once the instrument was on-orbit and operational, evaluation of the algorithms for success in signal detection, signal finding, and signal telemetry was undertaken. In response to the evaluation, updates have been made to optimize the data provided by the mission.

1. Introduction

The Ice, Cloud and land Elevation Satellite-2 (ICESat-2) has been providing global height measurements to the scientific community since 2018. ICESat-2 has similar scientific objectives as its predecessor mission, ICESat (Schutz et al. 2005), with a focus on using satellite laser altimetry to support climate variable monitoring as a window to understanding Earth's response to a changing climate. The primary instrument onboard ICESat-2 is the Advanced Topographic Laser Altimetry System (ATLAS) and is one of the most technically advanced space-borne lidar for Earth Science to date (Martino et al. 2019). ATLAS is a photon-counting lidar, sensitive to single photon reflections from the surface of the Earth. The photon-counting technology facilitates the use of lower laser energy, creating a scenario where multiple beams and higher laser repetition rates allow for greater spatial coverage and higher spatial resolution, both of which were implemented improvements based on operational realizations identified by the predecessor mission (ICESat) (Markus et al. 2017; Magruder et al. 2021. The high repetition rate (10kHz) provides higher along-track spatial resolution and the capability to capture fine scale features on the surface in time and space to meet requirements associated with dynamic processes in our Polar Regions. The multiple beam configuration allows for the discrimination between surface slope and true elevation change in the case of repeat measurements (Smith et al. 2020). ICESat-2 mission requirements are described by Markus et al. (2017) and successful completion of the requirements is summarized in Magruder et al., 2024 (Magruder et al. 2024).

The large data volume associated with a photon counting lidar was anticipated and the approach to onboard data management and signal processing techniques had to be altered from previous missions. It was understood and expected that ATLAS would exceed the normal X-band radio downlink capabilities and could require additional downlink station contacts (McGarry et al.

2021). The ICESat-2 Project Science Office (PSO) made the decision early in the pre-launch mission phase to focus on reducing the data volume onboard via processing algorithms and then determine if there was a need for more ground station access. The onboard algorithms that comprise the flight software (FSW) were designed to provide a sophisticated means for signal finding and data reduction. These functions are performed through inventive use of onboard signal processing, databases, and telemetry window selection across the diversity of global environments and surface types (Leigh et al. 2015; McGarry et al. 2021). Each component of the comprehensive FSW was created around the idea of having flexible parameterization to accommodate on-orbit adjustments, changes, and updates as the mission matured and discoveries of future, unanticipated needs are identified through the prime mission lifetime and into the extended mission timeline.

The majority of the data volume acquired by ATLAS during each orbit and between downlink opportunities occurs during daylight hours. This accumulation is due to the nature of photon-counting systems, as ALTAS is susceptible to solar background noise entering the system at the same wavelength to the ATLAS laser (532 nm). During the day the ambient background noise can exceed 10 MHz, which creates the need for noise mitigation processing in order to not violate the telemetry constraints associated with downlink bandwidth limitations. Whether noise or signal, ATLAS detects and records the time of arrival for every received photon creating a disparity among detection types based on an extremely low signal to noise ratio (Anthony J. Martino et al. 2019). These challenges created a need for optimizing onboard techniques for ensuring capture of the surface signal without possible data losses associated with overloading downlink opportunities.

The overarching requirements for the onboard receiver algorithm FSW are: 1) Keep the average

daily science telemetry data volume below 577.4 Gb/day, 2) Use the real time position and attitude solutions to guide the surface signal finding within 2 km horizontally and 250 m vertically for off-nadir angles between 0˚ and ±5˚(with capabilities up to ±10˚ off-nadir pointing after July 20, 2023), and 3) Select/find surface signal at least 90% of the time in regions of optically thin cloud cover, but not constrained by surface reflectivity, topography or solar elevation angle.

The utility of the receiver algorithms is to meet the volume constraints while capturing a complete and accurate altimetry signal of surface elevations. This is accomplished through several complementary functions that involve signal processing and functions that use a set of onboard databases of Earth elevations and topographic relief to inform where to look for true surface signal. Once the approximate surface is determined, the algorithm can align an appropriate telemetry window to ensure appropriate signal retention and successful data downlink. Comprehensive descriptions of the onboard receiver algorithm operations and capabilities are well described in the previous publications (Leigh et al. 2015; McGarry et al. 2021) but will be mentioned in the subsequent sections for completion.

This article provides an overview of changes that have been made to the ICESat-2 FSW and receiver algorithms since launch. The FSW updates have been made to enhance ICESat-2's usefulness across a wide range of earth observation topics, including measurements of blowing snow and coastal bathymetry. We provide an overview of FSW and then discuss each update and the impact on ICESat-2 data products and the applications to earth observation science.

1.1 Signal processing

The Photon Counting Electronics (PCE) cards operate on each pair of strong and weak beams. The PCEs record the transmit and receive times of photons for each ATLAS pulse. Using

the transmit and receive times the time of flight (TOF) can be calculated and used to generate coarse range values that are then used to produce histograms of photon arrival times. The histograms are aggregates of 200 consecutive laser shots, corresponding to an along-track distance of 140 m (or 0.02 s) (McGarry et al. 2021). The flight software uses the histograms to perform initial signal and background rate estimates to inform data downlink criteria.

For two of the three strong beams a portion of the laser energy is redirected back to the receiver channel instead of being transmitted to the surface. This laser pickoff, called the TEP (Transmitted Echo Path), is fixed relative to the time of laser fire from which it was generated, with the primary pulse peak time-of-flight around 18-19 ns. The TEP is only recorded when it falls within the range window (RW) for a given laser fire but allows the instrument to record the shape of the outgoing laser pulse, providing a means to monitor the health and data quality of ATLAS. It also facilitates the identification of deteriorated conditions, such as transmit/receive pulse slips and fine count swaps. The most recent TEP photons meeting certain quality criteria are carried onto the ATL03 data product as ancillary information (Neumann et al. 2019).

1.2 Databases and Telemetry window selection

The next signal finding step is performed on the detected photons that exist within the determined range window through a combination of software and hardware approaches. The primary function of this step is to determine the appropriately sized vertical telemetry band that will encompass the surface photon reflections and limit excess data volume caused by noise photons and be telemetered down to ground stations for further processing. The telemetry band is defined as the vertical extent for which detected photons (signal and noise) are downlinked. The RW is ultimately determined by an onboard digital elevation model (DEM) that contains the minimum and maximum elevations globally. These elevation grids are indexed by latitude and

longitude and meet the requirement of 150 m (3σ) accuracy (McGarry et al. 2021). The RW is constrained to a vertical maximum of 6 km that includes a ±250 m height margin. To meet this requirement the onboard DEM is actually comprised of a tertiary grid system of varying resolutions (1˚ x 1˚, 0.25˚ x 0.25˚, 0.05˚ x 0.05˚) to maintain that the relief (vertical distance between maximum and minimum elevation at a given geographical location) does not exceed 5500 m. The baseline for where the expected surface elevation can be found within the vertical window is derived from the void-filled SRTM (Shuttle Radar Topography Mission) product released by the CGIAR-CSI (Consortium for Spatial Information; SRTM-CGIAR (Jarvis et al. 2008)) for the mid-latitudes and other available DEMs outside of the SRTM latitudinal reach (e.g. Greenland Ice Mapping Project (GIMP), Bedmap2, Global Multi-resolution Terrain elevation Data (GMTED), and the Canadian Digital elevation Database (CDED)). The EGM2008 geoid is used to estimate the ocean surface elevations (Leigh et al. 2015).

The global relief database is the second type of database onboard ICESat-2. This DRM (digital relief model) establishes the elevation range surrounding the identified ground signal that is incorporated into the telemetry band calculation, along with padding and offset parameters. The DRM is assembled at a resolution of 0.25˚ x 0.25˚, and contains the maximum relief values across two length scales (140 m and 700 m) (Leigh et al. 2015). The DRM relief values overlay the signal bin representing the perceived or apparent ground, helping ascertain the number of adjacent bins to incorporate into the downlink telemetry, aside from the signal bin itself. Failing to include the DRM relief values could result in the omission of ground and canopy signals in rugged and/or vegetated regions from the downlinked data. The DEM and DRM databases were enhanced by incorporating global vegetation heights obtained from Simard et al. (2011) (Simard et al. 2011).

The third type of database onboard ICESat-2 is the Surface Reference Mask (SRM) and, like the DRM, is at a resolution of 0.25˚ x 0.25˚. The SRM classifies the surface type, as a means to define values of vertical (elevation) padding required for the telemetry window. This is used to accommodate (and mitigate) the uncertainties in the relief estimates and geolocation knowledge. The SRM also indicates if there is vegetation, and if there is coastline for each tile. The four possible surface types are land ice, sea ice, land, and ocean with precedence given in that order for mask cells that cover multiple surface types (McGarry et al. 2021).

2. Materials and Methods

As part of the ATLAS FSW, the receiver algorithms use several adjustable parameter files that allow modifications to the signal processing elements of the software to be updated without having to modify or update the underlying code of the FSW and receiver algorithms. Many of the parameters are determined as a function of either surface type, spot type (i.e. beam energy), or day or night conditions allowing for fine-tuned and discipline specific adjustments. The values are specified in a set of three parameter files. Each of the three onboard PCE detectors have an independent set of files, however all three PCE parameter files are synchronized to the same update version. The receiver algorithm parameter file types and their parameters that are frequently updated are described in the following sections.

2.1 “Knobs” files (nominal and alternate parameters)

The Knobs files contain parameters that allow control over the data volume by selecting content in the telemetry downlink and the conditions associated with when to telemeter data. Each PCE has a nominal Knobs file and an Alternate Knobs file. The nominal Knobs files are optimized for the main science objectives and keeping the data volume within the daily limit. The Alternate Knobs are used for those situations where the satellite is performing maneuvers

associated with ocean scans, round-the-world scans (Luthcke et al. 2021), and targets of opportunity (Magruder et al. 2021). The Alternate Knobs files create a configuration that continuously telemeters data regardless of surface type, time of day, or signal type. Only one Knobs file type is in use at a time for each PCE.

The telemetry "Knobs" parameters control what data to telemeter, or the content of the downlink. There are knobs for the numerous possible signal conditions, categorized by surface type, day or night acquisition, and spot strength (strong or weak). The No-signal Timer parameters count the number of consecutive Major Frames (nominally 200 laser pulses) to telemeter when no signal is identified by the receiver algorithms. There are two timer states, timer1 and timer2. The receiver algorithms enter the timer1 state when no signal is found for a major frame and the knobs are configured to still telemeter data. Timer1 currently varies from 10 to 50 major frames, depending on the surface type. Timer2 begins when timer1 has expired and currently varies from 100 major frames to no expiration, depending on the surface type. The timer2 state generally consists of vertically larger telemetry bands. If timer2 expires then no data is selected to telemeter until signal is found again.

2.2 PPR (Position, Pointing, and Range parameters)

The PPR files contain parameters associated with calculating each spot location on Earth and setting the Range Window (search area to look for signal). The Range Window Minimum Width parameters define the minimum allowed vertical width of the range window. It can be set separately for each surface type, day or night, and strong or weak spot.

2.3 ST (Signal and Telemetry parameters)

The ST files contain parameters used in signal processing and calculating the vertical width of the telemetry bands. The telemetry band padding parameters define the amount of

margin to add in the calculation of the telemetry band width. The padding value is doubled and added to the scaled relief to account for uncertainties in the relief value. The relief comes from the onboard DRM and the scale factor is a parameter in the ST file. The padding parameters are a function of surface type, spot type and relief value. There are four ranges of relief (R) values ($R \leq 189$ m, $189 \text{ m} < R \leq 567$ m, $567 \text{ m} < R \leq 1323$ m, $1323 \text{ m} < R$) which specify the interval of padding to use. Generally, the padding values increase with each interval, except for ocean surface types.

The telemetry band offset and padding parameters define the position and shape of the telemetry band in vertical space (Figure 1). Offsets can be applied to shift the telemetry band up or down, a positive offset shifts the telemetry band down in vertical space and a negative offset shifts the telemetry band up in vertical space. An offset of 0 centers the telemetry band around the signal location. Padding is applied based on the onboard DRM values and increases the overall height of the telemetry band (symmetrically around the signal position). Offset and padding can be applied independently or in concert with each other to achieve the necessary telemetry band.

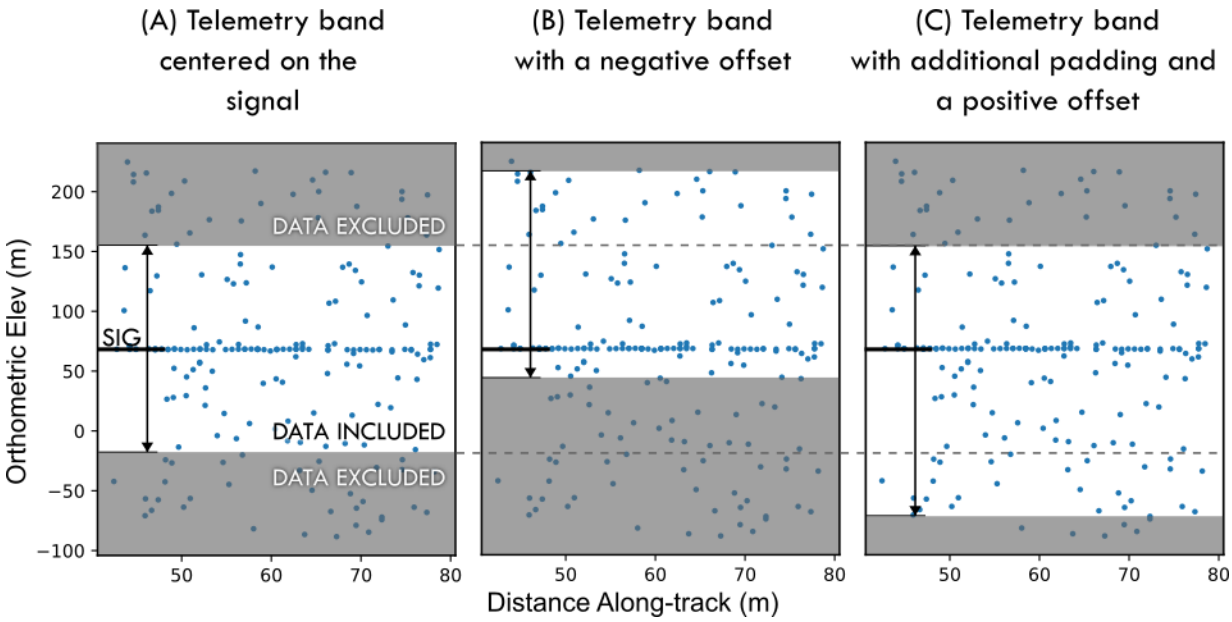

Figure 1. Diagram illustrating the different adjustments that are available when defining the telemetry window. 200-photon returns are illustrated in each plot and data that would be excluded (not downlinked) are shown in the gray boxes. (a) shows a normally centered telemetry window around a signal (ground surface) at ~60 m elevation, (b) the window with the same height as (a) with a negative offset applied to capture more data above the signal surface, and (c) increased padding applied and a positive offset to increase the amount of data below the signal surface while maintaining the height of the window limit above the signal.

3. Summary of on-orbit changes

Parameter file Versions 01 through 05 cover the work done in pre-launch simulated testing, Integration and Testing (I&T), and observatory testing. ICESat-2 launched on 15 September 2018 operating on Version 06 parameter files (McGarry et al., 2020). Since launch, there have been five version updates to the operational parameter files. As of this writing, ICEsat-2 is operating on Version 14. There are several file versions tested on-orbit or only in simulated testing that were never made operational (07, 09 and 12). Table 1 has a summary of the testing and operational timelines for each operational version since launch.

Table 1. Parameter file version test dates, test durations and operational start dates. Versions 07 and 09 were tested on-orbit, but never made operational. Version 12 was not tested on-orbit and is therefore excluded from the table. *Due to resetting of PCE1 and PCE3, there are gaps in usage of v14: 29 Dec 22 - 6 Feb 23 for PCE1 and 2 Feb 23 - 6 Feb 23 for PCE3.

Version	Test Start Date	Test Duration (approx.)	Date Operational	Description
06	--	--	15 Sept 2018	Launch version
07	4 Apr 2019	4 hours	--	Data enhancements (TEP crossing signal) Corrected range window settings
08	9 May 2019	5 hours	3 Sept 2019	Data enhancements (TEP crossing signal, ocean, blowing snow) Corrected range window settings
09	25 Oct 2019	2 days	--	Data enhancements (lake bathymetry)
10	17 Nov 2020	2 weeks	27 Jan 2021	Data enhancements (ocean bathymetry)
11	16 Feb 2021	3.5 hours	12 Mar 2021	Error mitigation related to range windows
13	18 May 2021	5 hours	1 June 2021	Data enhancements (weak spot ocean)
14	1 Nov 2022	30 days	1 Dec 2022 *	Data enhancements (coastline bathymetry)

3.1 Version 08: TEP Signal Crossing, Ocean and Blowing Snow Band Widths

The first operational version revision of the parameter files is Version 08 was tested on orbit in May 2019 and made operational on 3 September 2019. This version includes changes to the Knobs, PPR, and ST files. Version 08 updates incorporated three major changes: 1) mitigating the loss of data when the Transmitter Echo Path (TEP) is close to surface, which reduced the range window widths for non-TEP photons to the nominal value 2) increasing telemetry band widths to capture blowing snow and 3) increased telemetry band widths more area around the open ocean surfaces.

The first Knobs file update mitigates data losses when the TEP is close to an ocean or sea ice surface, shown in Figure 2 for the ocean. The nominal parameter settings tell the receiver

algorithms to ignore the area around the TEP (~27 meter vertical window) when searching for surface signal to avoid selecting the TEP as signal. This logic combined with the TEP approaching a flat surface can result in multiple Major Frames of missed surface data. In order to preserve signal data when the TEP intersects with the surface return, the Knobs parameters for the strong spots over ocean are turned on when no signal is found via the standard histogramming approach. The no-signal timer1 for both ocean and sea ice was reduced from 25 Major Frames to 10 Major Frames and the no-signal timer2 is set to continuously telemeter data. By switching to the no-signal timer2 state sooner, the telemetry bands are set to the width of the range window ensuring both the TEP and surface are captured until there is sufficient distance between the TEP and surface, on the order of approximately 20 m for ocean and sea ice. This approximation allows for the established histogram bin size of ~12 m for ocean or sea ice surface signal and ~27 m for the TEP. Assuming the surface signal is in the middle of the bin (6 m on each side) and the TEP is in the middle of the bin (14 m on each side) the result is the 20 m estimate but in general the range is ~14 m to ~24 m.

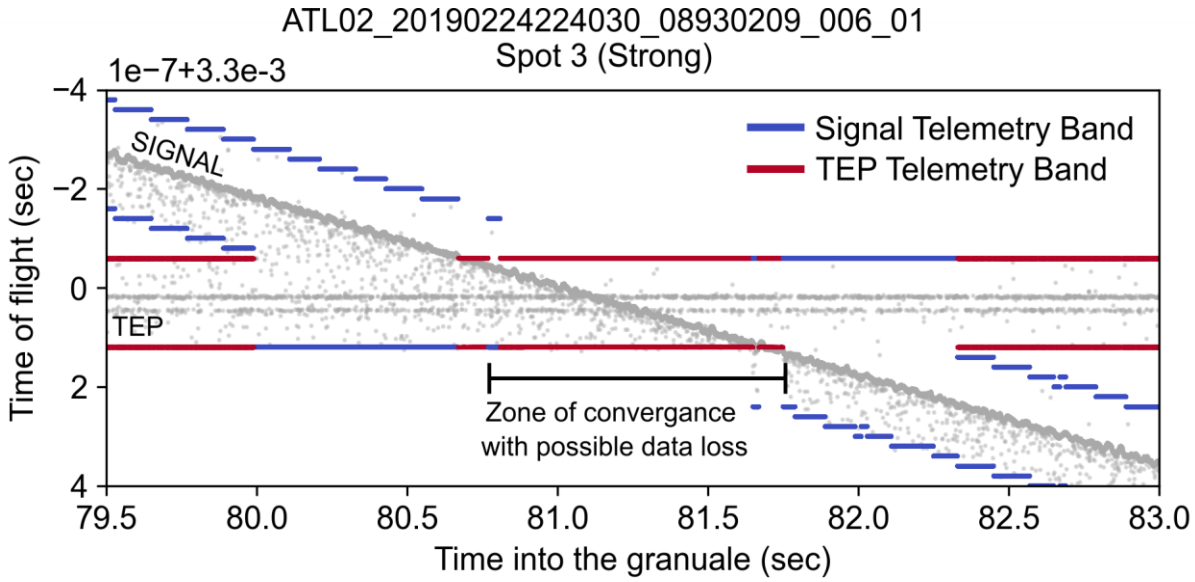

Figure 2. Due to the logic of handling the TEP within the receiver algorithms, some Major Frames clip the ocean surface as it converges with the TEP. At about 80.75 seconds and 81.75 seconds the ocean surface is right at the bounds of the telemetry band, which is centered about and sized for the TEP.

The second Knobs file update resolves an inconsistency between the receiver algorithms and the flight software by removing the 140 m scale relief data (DRM-140) as an option for the no-signal telemetry band relief in the timer2 state. The correct options for the no-signal telemetry band relief in the timer2 state are the DEM (the nominal setting) or the 700 m scale relief data (DRM-700). Note that both changes are replicated in the Alternate Knobs files where applicable. The launch version of the PPR parameter files force the range windows for strong spots over sea ice and land ice at night to a minimum of 5 km to capture the TEP. Because the TEP is only present in two of the six spots (#1 and #3), the 5 km range window width minimum setting for the remaining strong spot (#5) was reduced to the nominal minimum value of 500 meters.

At the request of the ICESat-2 Science Team, the telemetry band widths for the ocean, land ice and sea ice surface types were increased in the ST files. The ocean telemetry bands gain 20 meters in total by increasing the telemetry band padding parameter by 10 meters, resulting in

ocean telemetry bands of 48 m in vertical height (±24 m above and below the signal). The land ice and sea ice telemetry bands are extended upwards by 30 meters to better capture blowing snow. This is accomplished by increasing the telemetry band padding by 15 meters and applying a -15-meter offset.

3.2 Version 10: Ocean Bathymetry

Several ICESat-2 Science Team members have focused on understanding the bathymetric capabilities of ATLAS once on-orbit and it was discovered that there were areas of clipped bathymetry data in open ocean tracks. This was due to the variable nature of the telemetry band limits along the coastlines and in open ocean. Figure 3 shows an example in the Indian Ocean in the Seychelles where shallow reef bathymetry has been excluded by the telemetry band size constraints. Bathymetric returns generally reach to 30 m below the water surface, and occasionally to 50 m (Parrish et al. 2019).

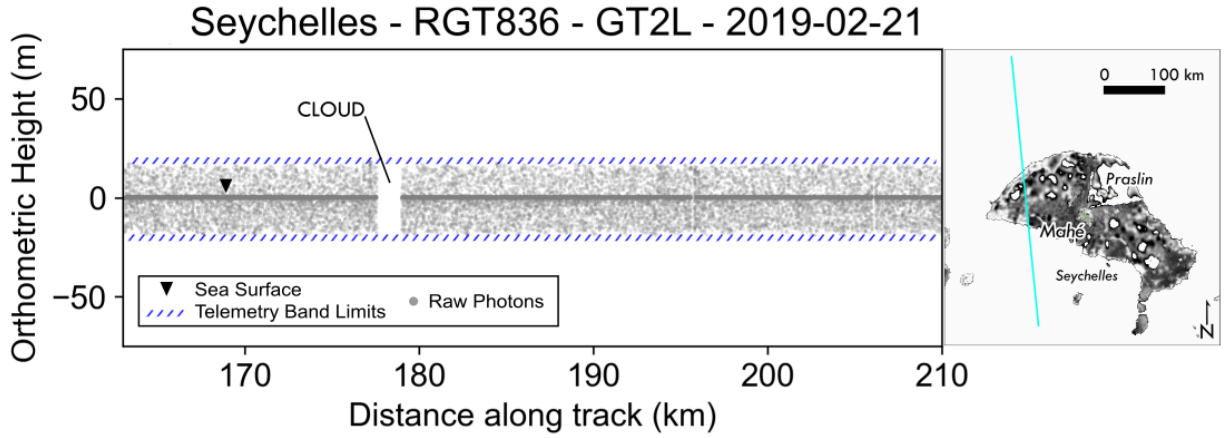

Figure 3. An open ocean ground track showing the pre-Version 10 update telemetry band limits in the Seychelles. The shallow reef system to the west of Mahe island has known bathymetry that is less than 50 m deep and should be retrievable by ICESat-2, but has been excluded from the data because of the telemetry band limits (used with permission from Dietrich et al., 2023).

Previously, the ocean telemetry bands spanned 48 m centered on the predicted surface, meaning they only reached 24 m below the surface. To reduce ocean bathymetry clipping, the

strong beam ocean telemetry bands were extended to reach at least 54 m below the surface by adjusting the padding and offset parameters. The vertical padding was increased by 15 m to 39 m and a vertical offset of +15 m is applied. The new padding and offset values extend the telemetry band deeper below the predicted surface while leaving the above surface limit unchanged. Utilizing the offset parameter allows for a smaller increase to the padding to extend to the desired depth, reducing the potential increase to the data volume. The padding and offset parameter changes are applied to the three strong spots and affect all ocean telemetry bands, not just areas with possible bathymetry (Dietrich et al. 2023).

Because the nominal parameters at the time of the version 10 update were set to not downlink weak spots data over oceans, no changes were made to the weak spot parameters because the weak spots are less likely to produce bathymetry (citations for less bathy in weak spots). A future (V13) update added the ability to telemeter weak spot ocean data., however the Version 10 changes for bathymetry capture are not applied as. The Alternate Knobs in version 10 allowed for weak spot data to be downlinked, but the weak spot ocean telemetry bands did not have the increased padding and offset settings used in the strong spots. For more details on receiver algorithm updates related to bathymetric data acquisition (Versions 10 and 14), see Dietrich et al. (2023).

3.3 Version 11: Range Window Error Mitigation

In late 2020, an issue was discovered in which certain alignments of a strong/weak pair of range windows can trigger an error in the Data Flow Controller (DFC) logic, called a transmit/receive pulse (Tx/Rx) slip. When a Tx/Rx slip occurs, the ATL02 product generation code detects and corrects the error as detailed in Martino et al. ((Martino et al. 2019), Section 2.5.7.3). In rare cases the error cannot be fixed with the current software, and the granule fails

before an ATL03 product file is generated. The error can be triggered at any time, but most frequently occurs when the range windows are forced “open”. In parameter file Versions 08 through 10, the range windows for spots 1 and 3 are set to a minimum width of 5000 m to increase the frequency that the TEP can be captured. By forcing the range window for these strong spots to be much wider than they may be otherwise, the starts of the strong and weak spot range windows are more frequently farther apart, conditions which increase the likelihood of triggering the error. This is further supported by the decreased frequency of the error for PCE3, which does not include TEP, and whose strong-weak pair always have equivalent range window width minimums.

To mitigate the issue, the PPR files are updated to no longer force the range windows for spots 1 and 3 over land ice and sea ice at night to a minimum of 5000 m. The range window width minimums are updated to the nominal value of 500 m. This change does not fix the DFC logic error, but is a mitigation measure to decrease the frequency at which the error can occur. Additionally, the return to science mode sequence was updated on 27 May 2021 to further decrease the frequency of the error.

3.4 Version 13: Ocean Weak Spots

Prior to the Version 13 updates, weak spot ocean data was telemetered only when the Alternate Knobs were in use. Users of the Ocean Elevation Along-track Data Product (ATL12) found that weak spot returns have a sufficient signal-to-noise ratio to detect the ocean surface (Yu et al. 2021) and requested weak beam data to be consistently downlinked over the ocean. The utility of weak spot ocean data is further supported by the routine use in ICESat-2 calibration scans which support spacecraft pointing and geolocation accuracy assessments (Luthcke et al. 2021). In the Knobs parameter files, the telemetry knobs for weak spot ocean

conditions were adjusted to downlink data when a Major Frame (nominally 200 pulses) or Super Frame (nominally 1000 pulses) signal is found. If no signal is found, then no data for weak spots is downlinked to minimize any increase in data volume. Note that the changes made in Version 13 do not extend the telemetry bands for bathymetry that were introduced in Version 10 for the strong spots. Version 13 parameters became operational on 1 June 2021.

3.5 Version 14: Coastline Bathymetry

The increased ocean telemetry bands in Version 10 reduce bathymetry clipping in the open ocean, but that did not mitigate all of the instances of missing or clipped bathymetry data along coastlines. Figure 4 shows an example off the coast of North Carolina where the receiver algorithms set the telemetry band limits based on the land parameters, resulting in a loss of bathymetry. Because the on-board SRM can have multiple surface types in a single tile it prioritizes land over ocean when both are present in a SRM tile. As mentioned previously, the surface type dictates the level of vertical padding parameters for the telemetered data. Telemetry bands along coastlines therefore use the adjacent land parameters and, in some cases, lack the extended depth applied to the ocean telemetry bands because of the low relief values in the DRM.

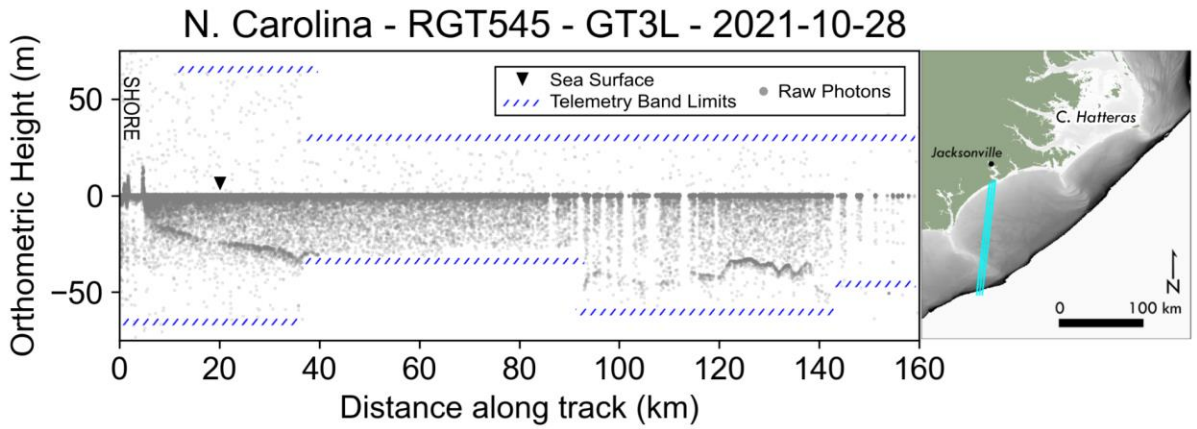

Figure 4. Bathymetric data loss after ocean telemetry band enhancements (v10) due to prioritization of land in the on-board SRM, near the coast of North Carolina. Until 90 km along track, the telemetry band parameters associated with land are in use when calculating the telemetry band limits. (used with permission from Dietrich et al., 2023)

To correct the telemetry band settings in coastal areas two important considerations had to be considered, the potential increases in data volume and reducing the likelihood of Did Not Finish Major Frame (DNF MF) conditions (data transfer errors from the PCE cards). To create the desired telemetry bands for coastal areas, the minimum padding over land for the strong spots was increased by 30 m to approximately 54 m. This padding applies to all land areas with a DRM relief value of 189 meters or less, highlighted in orange in Figure 5. The increase in the minimum land padding reduces bathymetry clipping along coastlines where the SRM has not yet switched from land to ocean. The changes are not applied to the weak spots, to remain consistent with the previous ocean updates for capturing bathymetry (Version 10 and 13). These updates became operational on-orbit on 1 December 2022. After this date, PCE1 and PCE3 each required resetting. The resets result in gaps in Version 14 usage starting on 29 December 2022 for PCE1 and 2 February 2023 for PCE3. Version 14 became the permanent nominal parameters on all PCEs on 6 February 2023.

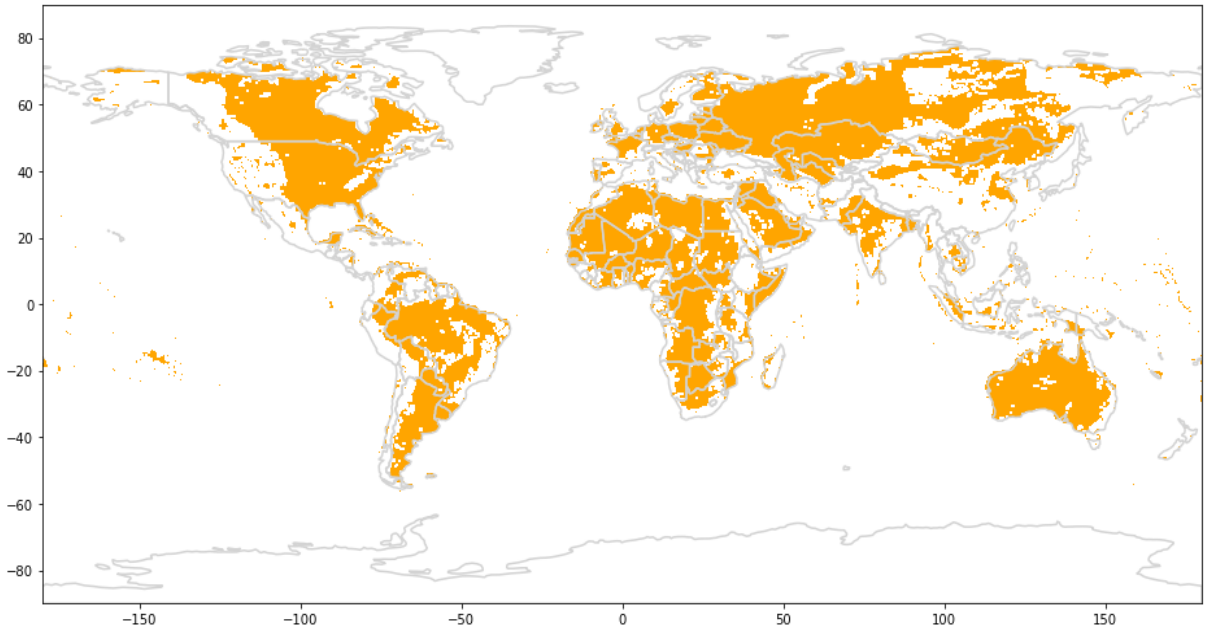

Figure 5. Map of DRM tiles where the increased land padding is applicable. These tiles have a relief range of 0 to 189 meters.

4. Results and Discussion

4.1 Version 08

Updates to the Knobs files in Version 08 mitigate the potential loss of data when the TEP crosses the ocean or sea ice surface due to the receiver algorithms' exclusion of the region about the TEP when searching for signal. When an ocean or sea ice surface enters the TEP region, the receiver algorithms enter the no-signal state and the updated Knobs are configured to continue telemetering the data using the no-signal state parameters. Figure 6 shows an example of the TEP crossing a sea ice surface. The Version 08 Knobs settings produce telemetry bands that successfully capture both the TEP and the surface as they intersect without any data clipping. When the surface enters the TEP region, the receiver algorithms first go into the no-signal timer1 state and telemeter 10 Major Frames centered about the last known signal. After timer1 concludes, the receiver algorithms switch to the no-signal timer2 state and telemeter bands that

span the entire range window, ensuring surface is contained within the telemetry band. Timer2 concludes once a signal is found outside the TEP region. It is possible that both TEP and clouds, or other noise features, are present in the range window. In such cases, noise features may be selected as signal to be telemetered along with the TEP, and surface signals may be missed.

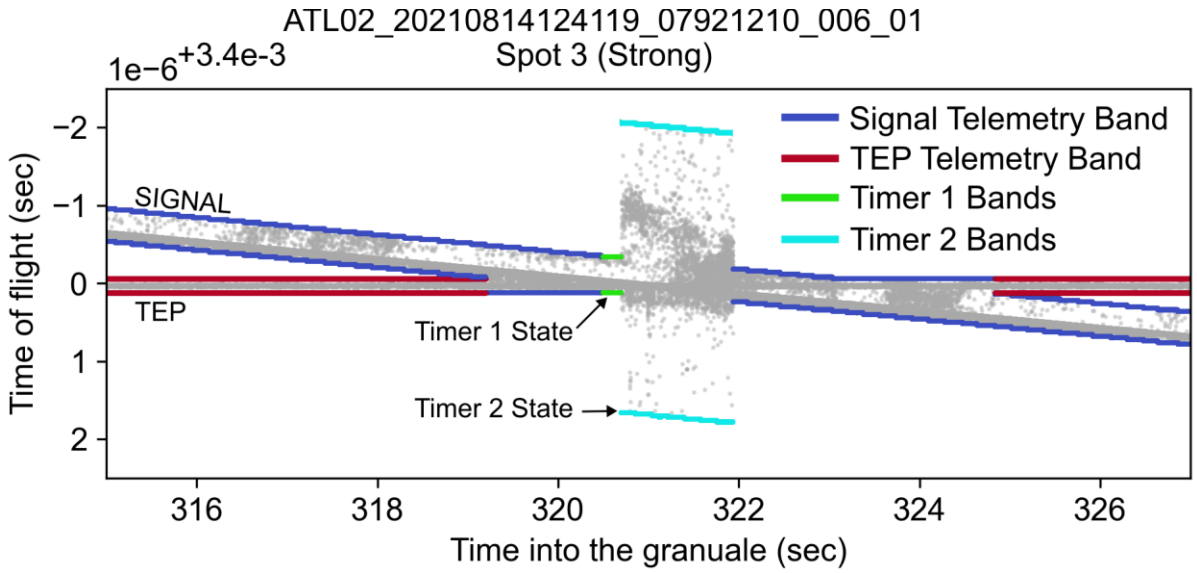

Figure 6. Example showing how the Version 8 changes for how the telemetry bands are calculated for areas containing surface signal and TEP convergence.

As the telemetry bands containing the surface signal (blue) and the telemetry bands containing the TEP (red) converge, they first are combined into one telemetry band for each Major Frame until the TEP is close enough to trigger the no-signal states, as shown in Figure 6. For ten Major Frames the telemetry bands in the no-signal timer1 state (green) which are centered on the last known signal location followed by over one second worth of the telemetry bands in the no-signal timer2 state (cyan), which are centered within the range window. The telemetry bands go back to a combined TEP and signal band once the signal is sufficiently out of the TEP region until they are far enough apart to be telemetered separately.

The second update in Version 8 increased the telemetry band padding and offset parameter updates in the ST files for land ice and sea ice to increase the above surface portion of the telemetry band to better capture blowing snow. Blowing snow is an important component to understanding surface-atmosphere energy flux particularly in the polar regions (Herzfeld et al. 2021) and this parameter change accommodates further investigations into these processes. All land ice and sea ice telemetry bands after the Version 08 update have an additional 30 meters in vertical width applied above the surface telemetry band limit, leaving the below surface limit unchanged, as described in Section 2. The total height above the surface in the telemetry band varies based on the relief value in the DRM. Figure 7 shows data from a portion of the same reference ground track in Antarctica (land ice) before and after Version 08 is made operational. The range in telemetry band widths increased by 30 meters, from 57 - 63 meters to 87 - 93 meters. The surface is no longer centered in the telemetry band in Figure 7B since the additional 30 meters of padding is expressed in the upper telemetry band limits.

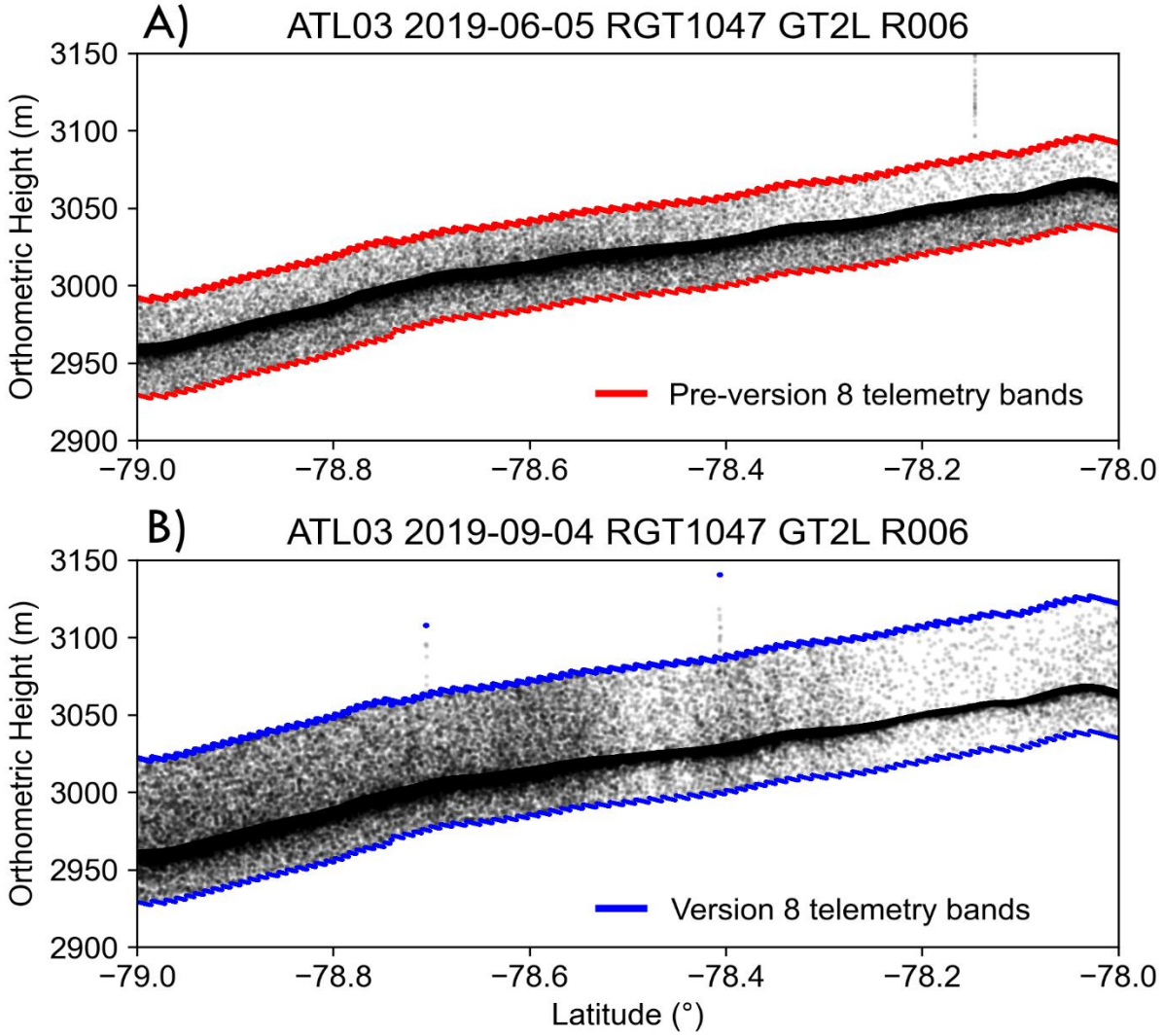

Figure 7. Areas of blowing snow in Antarctica before (A) and after (B) the Version 08 updates become operational. (A) On June 5, 2019, blowing snow is captured within the telemetry bands, which have a vertical width ranging from approximately 57 to 63 meters. The surface signal is centered within the telemetry bands, resulting in approximately 29.5 to 31.5 meters above the surface available to capture blowing snow. (B) On September 4, 2019, additional blowing snow is captured within the telemetry bands. The Version 08 updates produce telemetry bands with a vertical width ranging from 87 to 93 meters with the additional 30 meters only applied to above the surface. This results in approximately 59.5 to 61.5 meters of space above the surface to capture blowing snow.

The third update implemented in Version 8 included small adjustments to telemetry bands for the ocean surface type. The telemetry band padding parameter was increased to create a total vertical band height of 48 m in vertical height (±24 m around the signal) (Figure 8).

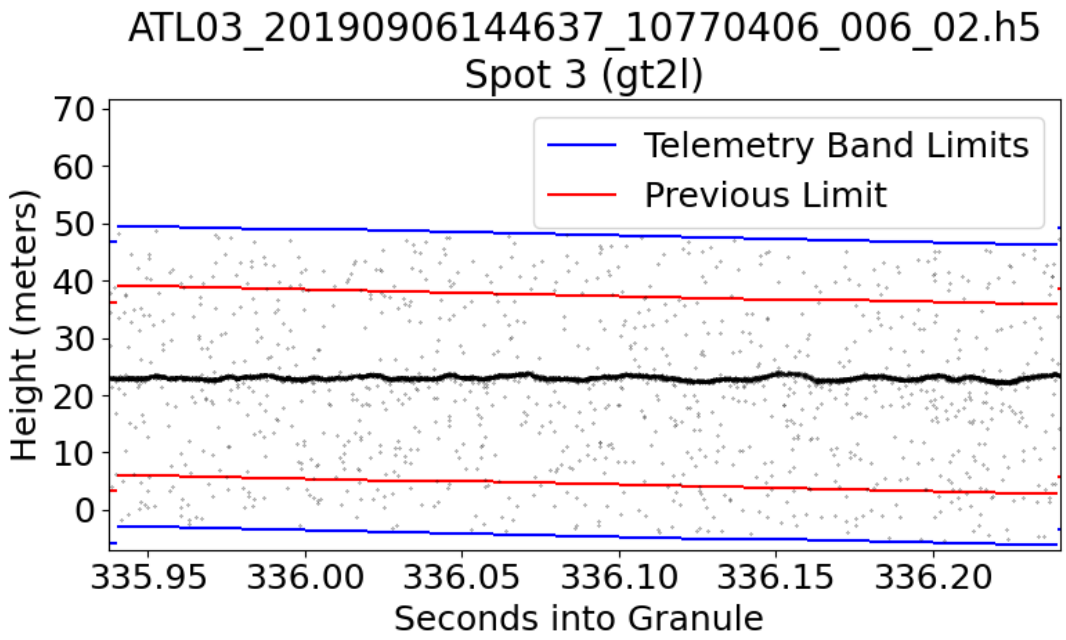

Figure 8. Telemetry over the ocean after the increase to the ocean telemetry band padding parameters. The Version 08 telemetry bands (blue) span a vertical width of ~51 meters, gaining ~10 meters both above and below the surface compared to the telemetry band limits prior to Version 08 (red).

4.2 Version 10

By extending the strong spot telemetry bands over ocean to 54 meters below the surface, bathymetry previously excluded in the data can now be captured. More specifically, potential bathymetry that falls below the previous telemetry band lower limit of 24 meters below the surface to the updated lower limit of 54 meters is now included in the downlinked data. Figure 9 shows an example near the Seychelles where potential bathymetry is captured in the extended portion of the telemetry band. See Dietrich et al. (Dietrich et al. 2023) for additional details and examples.

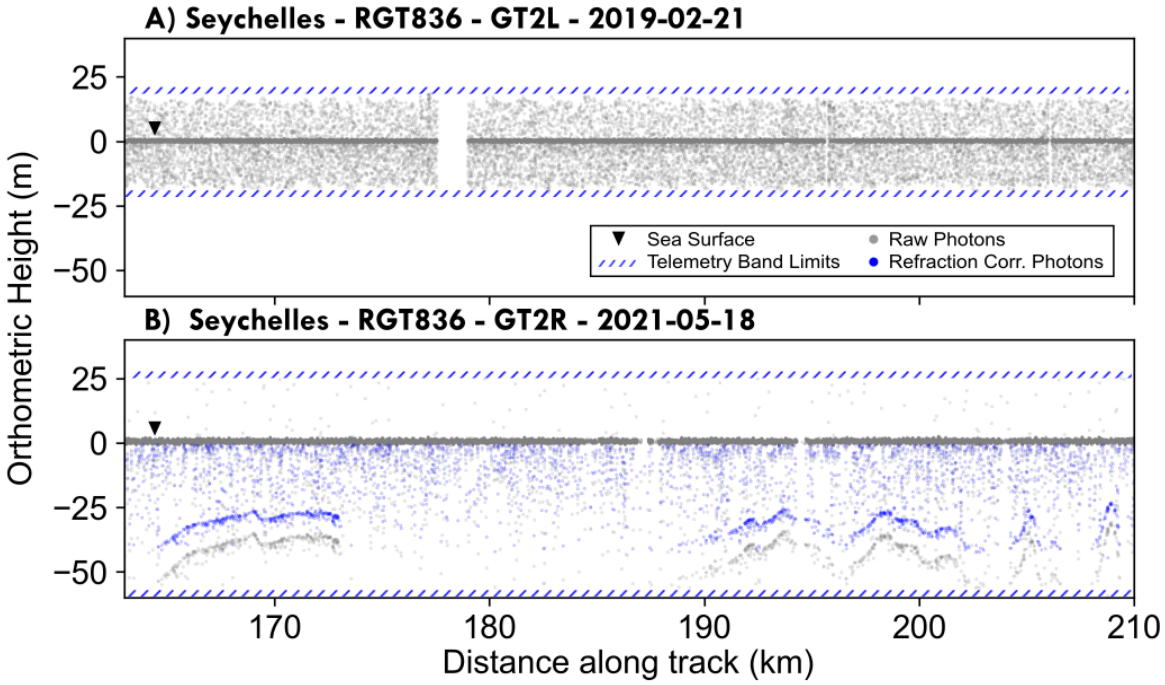

Figure 9. Telemetry bands for reference ground track (RGT) 0836 in the Seychelles. a) illustrates the telemetry bands before the Version 10 update showing no bathymetry. b) highlights the expanded telemetry bands of Version 10 and the newly available reef bathymetry that was previously not recorded (used with permission from Dietrich et al., 2023).

4.3 Version 11

The range window settings in Version 08 introduced, at times, large differences in the range window starts of strong-weak pairs for PCEs 1 and 2. These differences are often on the order of 2 kilometers or more. As described above, this condition increases the likelihood of Tx/Rx slips. The range window adjustments in Version 11 reduce the differences in range window starts to an average of a few meters or less, consistent with measurements for PCE 3.

The Version 11 mitigation successfully reduced the conditions favorable for TxRx slips introduced in Version 08. In Versions 08 through 10, TxRx slips occurred in 1,759 granules, or 1.54% of data over ~1.5 years. After the Version 11 update, TxRx slips occurred in just 314 granules, or 0.15% of data over more than 2.5 years as of this writing. Note that these figures consider only the most common TxRx slip type, corrected in ATL02 (A. Martino, Field, and

Ramos-Izquierdo 2020).

4.4 Version 13

Version 13 became operational on June 1, 2021, greatly increasing the amount of weak spot data available over the open oceans. Figure 10 shows the daily number of weak spot, ocean photons with high signal confidence in ATL03 (Neumann et al. 2019) for 1 May and 31 June 2021, with a distinct jump on June 1, 2021 when Version 13 became operational. The ATL03 weak spot, ocean data for May 2021 were data that were collected when the Alternate Knobs are in use (17 ocean scans, 8 round-the-world scans, and parts of the 42 ocean targets of opportunity (TOOs)) and times when the on-board SRM classification of ocean does not align with the ATL03 surface type classification. Because June 2021 has only one additional ocean scan and round-the-world scan, the increase in high signal confidence weak spot, ocean data can be attributed to the Version 13 parameter update. The addition of weak spot, ocean telemetry increases its fraction of the total data telemetered by approximately 1%. This small increase in percentage of data telemetered is expected due to the small size of the telemetry band (48 meters) and the reduced photon rate for weak-spots.

A recent example of the utility of using the weak beam data is the recovery of ocean wave characteristics, particularly nearshore where the dynamics are more complex. Understanding wave direction and the overall geometry of wave motion is only possible with the correlation of signal between two beams, in this case a pair (Dietrich, Magruder, and Holwill 2023). It is anticipated that the inclusion of the weak spot will foster more science discovery moving forward as the mission accumulates data in relevant locations and extends coverage.

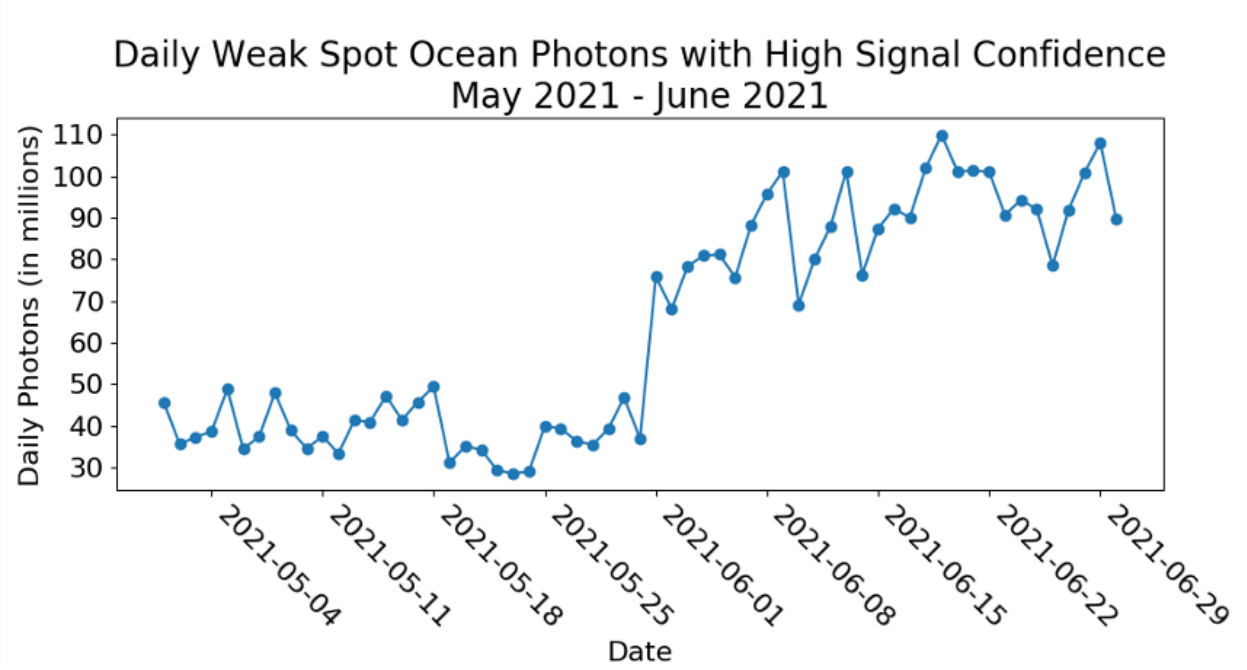

Figure 10. Daily sum of high signal weak spot, ocean photons in ATL03 from 05/01/2021 to 06/30/2021. The step increase in weak spot, ocean signal photons apparent on 06/01/2021 is due to the Version 13 update becoming operational.

4.5 Version 14

The majority of the bathymetry potentially observable by ICESat-2 falls along coastlines where the receiver algorithms set the telemetry band limits based on the parameters corresponding to land surface type. The Version 10 updates include only parameters corresponding to ocean surface type, so a large portion of potential bathymetry was not captured by those updates. The Version 14 updates extend the land telemetry bands to at least as deep as the ocean bands for areas that have a relief value less than or equal to 189 meters from the DRM. Figure 11b shows the effect of the version 14 updates compared to the previous band limits (Figure 11a and Figure 4). See Dietrich et al. (Dietrich et al. 2023) for a detailed study on how much additional potential bathymetry the Version 14 and Version 10 updates provide.

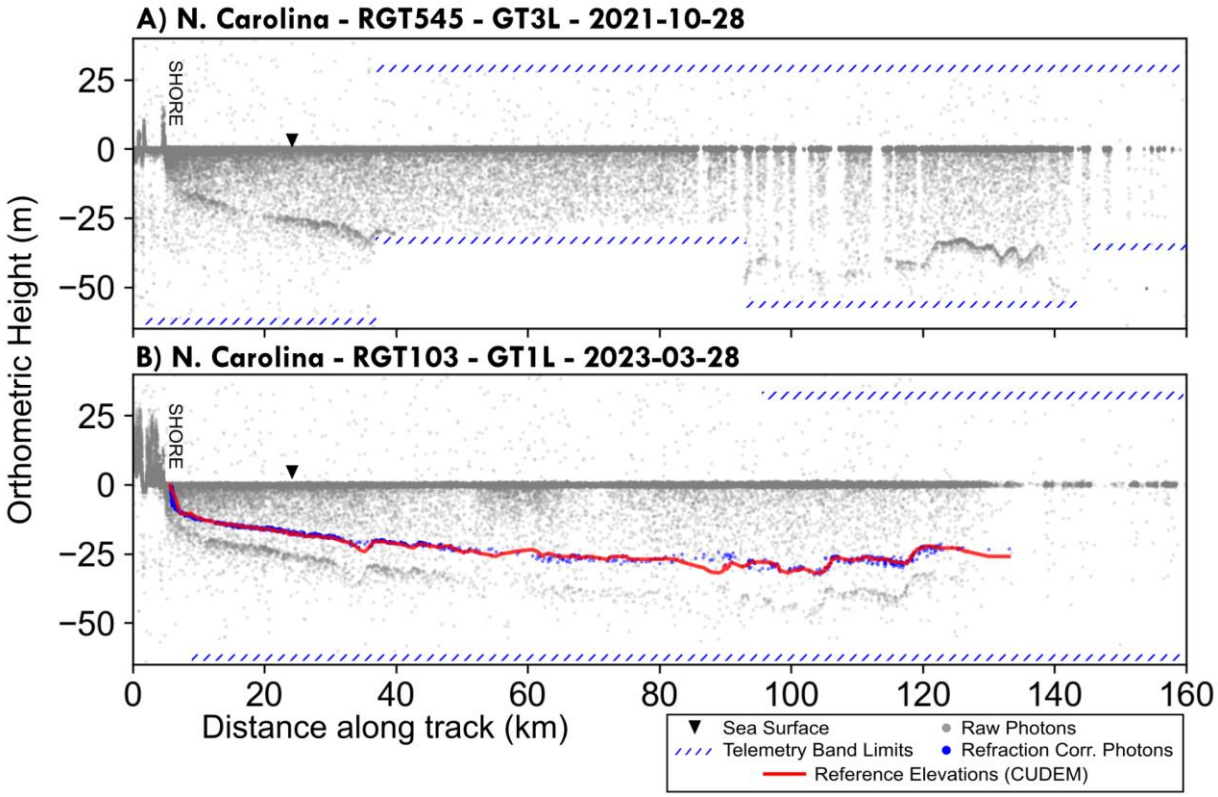

Figure 11. Newly available bathymetry off the coast of North Carolina, USA after the Version 14 update. a) Previous telemetry band limits highlighting the clipped bathymetry caused by the switching from land to ocean surface parameters and b) newly available continuous bathymetric profile made possible by the consistent lower telemetry band limit of -54 meters below the surface. Refraction corrected photon elevations are shown in blue with a comparison to NOAA CUDEM elevations. (used with permission from Dietrich et al., 2023)

6. Conclusions

The ICESat-2/ATLAS receiver algorithms have had several updates since the launch of the satellite in 2018. These modifications were motivated by a desire to optimize (further) the science that the ICESat-2 measurements are able to facilitate and also to mitigate some operational issues. This paper is a result of many scientists and engineers evaluating the icesat-2 data and highlights the exceptional response of the ICESat-2 project office to providing the scientific community the quality of data that meets multi-disciplinary standards despite not being part of the prime mission objectives. It is expected that these new adjustments and

accommodations will allow for enhanced research and discovery in many areas of Earth science. The software changes onboard were possible because of the careful planning and insight of the ATLAS engineers to enable adjustments to the quantity and quality of signals collected. ICESat-2 is an example of adaptability and resilience on-orbit to ensure that the mission is optimized for data collection that maximizes the scientific return.

Acknowledgments

The authors wish to thank the ICESat-2 Project Science Office for the support as well as the NASA HQ support under grant #80NSSC23K0044. We also thank Alvaro Ivanoff for the data volume statistics around the Version 13 update and related figure.

Data Availability

All data used in this publication is publicly available from the National Snow and Ice Data Center (https://nsidc.org/) from ATL02 and ATL03 ICESat-2 data products.

References

Dietrich, James, Lori Magruder, and Matthew Holwill. 2023. "Monitoring Coastal Waves with ICESat-2." *Journal of Marine Science and Engineering* In pre-print. https://doi.org/Doi: 10.20944/preprints202310.1185.v1.

Dietrich, James, Ann R Rackley Reese, Aimée Gibbons, Lori A. Magruder, and Christopher Parrish. 2023. "Analysis of ICESat-2 Data Acquisition Algorithm Parameter Enhancements to Improve Worldwide Bathymetric Coverage." Preprint. Preprints. https://doi.org/10.22541/essoar.169447414.45310708/v1.

Herzfeld, Ute, Adam Hayes, Stephen Palm, David Hancock, Mark Vaughan, and Kristine Barbieri. 2021. "Detection and Height Measurement of Tenuous Clouds and Blowing Snow in ICESat-2 ATLAS Data." *Geophysical Research Letters* 48 (17). https://doi.org/10.1029/2021GL093473.

Jarvis, A., Hannes Reuter, Andy Nelson, and Edith Guevara. 2008. "Hole-Filled SRTM for the Globe Version 3, from the CGIAR-CSI SRTM 90m Database." *See Http://Srtm. Csi. Cgiar. Org*, January.

Leigh, Holly W., Lori A. Magruder, Claudia C. Carabajal, Jack L. Saba, and Jan F. McGarry. 2015. "Development of Onboard Digital Elevation and Relief Databases for ICESat-2." *IEEE Transactions on Geoscience and Remote Sensing* 53 (4): 2011–20. https://doi.org/10.1109/TGRS.2014.2352277.

Luthcke, S. B., T. C. Thomas, T. A. Pennington, T. W. Rebold, J. B. Nicholas, D. D. Rowlands, A. S. Gardner, and S. Bae. 2021. "ICESat-2 Pointing Calibration and Geolocation

Performance." *Earth and Space Science* 8 (3). https://doi.org/10.1029/2020EA001494.
Magruder, Lori, Kelly Brunt, Thomas Neumann, Bradley Klotz, and Michael Alonzo. 2021. "Passive Ground-Based Optical Techniques for Monitoring the On-Orbit ICESat-2 Altimeter Geolocation and Footprint Diameter." *Earth and Space Science* 8 (10). https://doi.org/10.1029/2020EA001414.
Magruder, Lori, Thomas Neumann, and Nathan Kurtz. 2021. "ICESat-2 Early Mission Synopsis and Observatory Performance." *Earth and Space Science* 8 (5). https://doi.org/10.1029/2020EA001555.
Magruder, Lori, Tom Neumann, Nathan Kurtz, and Tyler Sutterley. 2024. "The Ice, Cloud and Land Elevation Satellite-2: Meeting the Prime Misison Science Requirements." *Remote Sensing of Environment*, no. In review.
Markus, Thorsten, Tom Neumann, Anthony Martino, Waleed Abdalati, Kelly Brunt, Beata Csatho, Sinead Farrell, et al. 2017. "The Ice, Cloud, and Land Elevation Satellite-2 (ICESat-2): Science Requirements, Concept, and Implementation." *Remote Sensing of Environment* 190 (March): 260–73. https://doi.org/10.1016/j.rse.2016.12.029.
Martino, A. J., M. R. Bock, R. L. Jones III, T. A. Neumann, D. Hancock, P. W. Dabney, and C. E. Webb. 2019. "ATLAS/ICESat-2 L1B Converted Telemetry Data, Version 1." NASA National Snow and Ice Data Center Distributed Active Archive Center. https://doi.org/10.5067/ATLAS/ATL02.001.
Martino, Anthony, Christopher T Field, and Luis Ramos-Izquierdo. 2020. "ICESat-2/ATLAS Instrument Linear System Impulse Response." Preprint. Geophysics. https://doi.org/10.1002/essoar.10504651.1.
Martino, Anthony J., Thomas A. Neumann, Nathan T. Kurtz, and Douglas McLennan. 2019. "ICESat-2 Mission Overview and Early Performance." In *Sensors, Systems, and Next-Generation Satellites XXIII*, 11151:68–77. SPIE. https://doi.org/10.1117/12.2534938.
McGarry, J. F., C. C. Carabajal, J. L. Saba, A. R. Reese, S. T. Holland, S. P. Palm, J.-P. A. Swinski, J. E. Golder, and P. M. Liiva. 2021. "ICESat-2/ATLAS Onboard Flight Science Receiver Algorithms: Purpose, Process, and Performance." *Earth and Space Science* 8 (4). https://doi.org/10.1029/2020EA001235.
Neumann, Thomas A., Anthony J. Martino, Thorsten Markus, Sungkoo Bae, Megan R. Bock, Anita C. Brenner, Kelly M. Brunt, et al. 2019. "The Ice, Cloud, and Land Elevation Satellite – 2 Mission: A Global Geolocated Photon Product Derived from the Advanced Topographic Laser Altimeter System." *Remote Sensing of Environment* 233 (November): 111325. https://doi.org/10.1016/j.rse.2019.111325.
Parrish, Christopher E., Lori A. Magruder, Amy L. Neuenschwander, Nicholas Forfinski-Sarkozi, Michael Alonzo, and Michael Jasinski. 2019. "Validation of ICESat-2 ATLAS Bathymetry and Analysis of ATLAS's Bathymetric Mapping Performance." *Remote Sensing* 11 (14): 1634. https://doi.org/10.3390/rs11141634.
Schutz, B. E., H. J. Zwally, C. A. Shuman, D. Hancock, and J. P. DiMarzio. 2005. "Overview of the ICESat Mission." *Geophysical Research Letters* 32 (21): L21S01. https://doi.org/10.1029/2005GL024009.
Simard, Marc, Naiara Pinto, Joshua B. Fisher, and Alessandro Baccini. 2011. "Mapping Forest Canopy Height Globally with Spaceborne Lidar." *Journal of Geophysical Research* 116 (G4): G04021. https://doi.org/10.1029/2011JG001708.
Smith, Ben, Helen A. Fricker, Alex S. Gardner, Brooke Medley, Johan Nilsson, Fernando S. Paolo, Nicholas Holschuh, et al. 2020. "Pervasive Ice Sheet Mass Loss Reflects

614 Competing Ocean and Atmosphere Processes." *Science* 368 (6496): 1239–42.
615 https://doi.org/10.1126/science.aaz5845.
616 Yu, Yao, David T Sandwell, Sarah T Gille, and Ana Beatriz Villas Bôas. 2021. "Assessment of
617 ICESat-2 for the Recovery of Ocean Topography." *Geophysical Journal International*
618 226 (1): 456–67. https://doi.org/10.1093/gji/ggab084.
619